

Rapid calculation of side chain packing and free energy with applications to protein molecular dynamics

J.M. Jumper^{1, a)} K.F. Freed^{2, b)} and T.R. Sosnick^{3, c)}

¹⁾*Department of Chemistry, University of Chicago*

²⁾*Department of Chemistry, James Franck Institute, University of Chicago*

³⁾*Department of Biochemistry and Molecular Biology, Institute for Biophysical Dynamics, University of Chicago*

(Dated: 2 February 2022)

To address the large gap between time scales that can be easily reached by molecular simulations and those required to understand protein dynamics, we propose a rapid self-consistent approximation of the side chain free energy at every integration step. In analogy with the adiabatic Born-Oppenheimer approximation for electronic structure, the protein backbone dynamics are simulated as preceding according to the dictates of the free energy of an instantaneously-equilibrated side chain potential. The side chain free energy is computed on the fly, allowing the protein backbone dynamics to traverse a greatly smoothed energetic landscape. This results in extremely rapid equilibration and sampling of the Boltzmann distribution. Because our method employs a reduced model involving single-bead side chains, we also provide a novel, maximum-likelihood method to parameterize the side chain model using input data from high resolution protein crystal structures. We demonstrate state-of-the-art accuracy for predicting χ_1 rotamer states while consuming only milliseconds of CPU time. We also show that the resulting free energies of side chains is sufficiently accurate for *de novo* folding of some proteins.

I. INTRODUCTION

Two major challenges must be overcome in order to accurately simulate protein dynamics. The first is the necessity of balancing the large and competing sources of energy and entropy whose sum determines both the thermodynamics and the native conformation of the protein. The second challenge involves the intensive sampling required to obtain a Boltzmann ensemble of conformations. The sampling challenge is addressed here by integrating out the side chain degrees of freedom to produce a coarse-grained configuration defined just in terms of the backbone N, C $_{\alpha}$, and C atoms. Consequently, backbone motions evolve on a smoother coarse-grained free energy surface with greatly reduced side chain rattling (molecular friction) compared to that for standard all-atom molecular dynamics simulations.

The uncertainty in the position of coarse-grain interactions heightens the difficulty of accurately parameterizing a coarse-grained model to represent the physical interactions. Moreover, all-atom force fields produce conformations that deviate from experiment, especially for unfolded proteins¹. We do not follow the customary process of matching the energies of the coarse-grained model to approximate the already inexact energies of atomistic force fields or try to interpret raw statistics for the distribution of interatomic distances in the Protein Data Bank (PDB)² through a reference state³. Instead, our side chain energies are determined as those that best repro-

duce the side chain conformations observed in the PDB when using the native-state backbone configurations.

This maximum-likelihood approach has key advantages: (1) it directly provides an interpretation of the structural information as a sample from the statistical mechanical ensemble of side chain packing, and (2) it can be evaluated quickly since we show that approximating the Boltzmann distribution for the side chains in a fixed backbone configuration does not require laborious discrete sampling of the χ angles in the side chain. Our method enables rapidly equilibrating coarse-grained simulation that can nonetheless contain significant molecular detail.

While the overarching goal of our work is preparation for extremely rapid molecular dynamics, our new interaction model gives very accurate and rapid predictions of side chain χ_1 angles. Using our side chain ensembles, we are able to predict χ_1 rotamer configurations with accuracy exceeding the state of the art from SCWRL4⁴, yet our predictions take less than 1% of the computational time. We also exceed the performance of the rapid side chain packing algorithm RASP⁵ by more than an order of magnitude. The accuracy of our side chain rotamer predictions validates that our side chain interaction potential captures important physics for side chain interactions, suggesting suitability for molecular dynamics.

The software for our side chain packing and molecular dynamics methods is open source. The source code may be obtained at <https://github.com/John-Jumper/Upside-MD>, where the version tagged `sidechain.paper` should be used to reproduce the results of this paper.

^{a)}jumper@uchicago.edu

^{b)}freed@uchicago.edu

^{c)}trsosnic@uchicago.edu

II. UPSIDE MODEL AND SIDE CHAIN FREE ENERGY EVALUATION

The positions of the N, C $_{\alpha}$, and C atoms constitute the backbone trace. The trace determines the fold of the protein, and the free energy of the trace is likely to preserve the major barriers that determine the long-timescale degrees of freedom in the protein. The strategy in our Upside model is to perform dynamics simulations of the backbone trace, while still including sufficient structural details (side chain structures and free energies, etc.) necessary to compute realistic forces on the three atoms of the backbone trace. The inclusion of the side chain free energy, rather than the side chains themselves, greatly smooths the potential governing the dynamics of the backbone trace, especially because of the reduction of steric rattling.

One can consider a representation of the protein configurations in terms of the coordinates $(\{b_i\}, \{\chi_i\})$ where b_i represents the positions of the backbone N, C $_{\alpha}$, and C atoms on the i -th residue and χ_i represents the side chain χ -angles on the i -th residue. Since bond lengths and angles are approximately constant for proteins, the positions of the protein atoms can be reconstructed with high accuracy from the $(\{b_i\}, \{\chi_i\})$ coordinates. Given a potential energy $V(\{b_i\}, \{\chi_i\})$, we define the free energy as a function of the backbone configuration,

$$\bar{V}(\{b_i\}) = -\log \int d\chi_1 \cdots d\chi_N e^{-V(\{b_i\}, \{\chi_i\})}. \quad (1)$$

Natural energy units are used so that $k_B T = 1$. An intermediate step of this derivation requires the introduction of a discrete approximation $\{\tilde{\chi}_i\}$ for our χ -angles and a discrete approximation $\bar{V}(\{b_i\}, \{\tilde{\chi}_i\})$ for the potential.

Rather than directly calculate Eq. 1, we define an intermediate discrete approximation to \bar{V} that is amenable to approximation techniques. Consider a discrete coarse-graining function g so that $\tilde{\chi}_i = g(\chi_i)$, where $\tilde{\chi}_i$ is a state label ($\tilde{\chi}_i \in \{1, \dots, 6\}$ as each side chain is represented by a bead located at one of up to 6 positions). The coarse-grain potential \tilde{V} is defined so that

$$e^{-\tilde{V}(\{b_i\}, \{\tilde{\chi}_i\})} \approx \int d\chi_1 \cdots d\chi_N \left(\prod_i \delta_{\tilde{\chi}_i f(\chi_i)} \right) e^{-V(\{b_i\}, \{\chi_i\})}. \quad (2)$$

In principle, any coarse-grain function for the side chains may be used. The discrete form \tilde{V} to the potential provides an accurate approximation as the distribution of χ -angles is sharply peaked (in the true potential V) within each discrete state $\tilde{\chi}$. See Figure S1 for an example of a function and section S4 where an optimized function f is derived. We make the following assumptions on the form of \tilde{V} . First, we assume an explicit function $y_i(b_i, \tilde{\chi}_i)$ exists for the side chain coordinates based only on the backbone coordinates and side chain state for residue i . We may relax the requirement to consider a single residue's

backbone position, but it is required that y_i depend on only a single side chain state $\tilde{\chi}_i$. These directed coordinates are approximately side chain centers of mass with direction given by the C $_{\beta}$ -C $_{\gamma}$ bond vector. A further assumption is that \tilde{V} can be expressed in the form

$$\begin{aligned} \tilde{V}(\{b_i\}, \{\tilde{\chi}_i\}) = & V^{\text{backbone}}(\{b_k\}) + \\ & \sum_i V_i^{(1)}(\{b_k\}, \tilde{\chi}_i, y_i(b_i, \tilde{\chi}_i)) + \\ & \sum_{i,j} V_{ij}^{(2)}(y_i(b_i, \tilde{\chi}_i), y_j(b_j, \tilde{\chi}_j)), \end{aligned} \quad (3)$$

where the pair interaction $V_{ij}^{(2)}(y_i, y_j) = 0$ for the side chain is taken to vanish beyond a cutoff R_{cutoff} . The dependence of the potential on the backbone is completely general, but the potential is assumed to contain at most a pairwise dependence on the discrete rotamer states $\tilde{\chi}_i$. Explicit parameterizations for y_i and \tilde{V} are defined in Section IV using the principle of maximum likelihood.

One can simulate the Boltzmann ensemble for \tilde{V} using molecular dynamics for the backbone $\{b_i\}$ and Monte Carlo moves for the side chain states $\{\tilde{\chi}_i\}$. But the strong steric interactions are likely to lead to slow equilibration and dynamics for both the side chains and backbone. Because we are predominantly interested in backbone motions, we return to the free energy \bar{V} in Eq. 1, now summing over discrete side chain states instead of integrating over continuous side chain angles,

$$e^{-\bar{V}(\{b_i\})} \approx \sum_{\tilde{\chi}_1, \dots, \tilde{\chi}_N} e^{-\tilde{V}(\{b_i\}, \{\tilde{\chi}_i\})}. \quad (4)$$

The potential \bar{V} represents a further coarse-graining of the system by completely replacing the influence of the side chains with a potential describing their adiabatic free energy for a given fixed backbone conformation. Because \bar{V} depends only on the (continuous) backbone coordinates, this choice of \bar{V} enables running standard molecular dynamics simulations instead of a hybrid of Monte Carlo and molecular dynamics.

Importantly, the potential \bar{V} is a much smoother function of the backbone coordinates than the original $V(\{b_i\}, \{\chi_i\})$ because the replacement of the side chain degrees of freedom with the approximate free energy of the side chains greatly reduces steric rattling and molecular friction. The reduction of the ruggedness of the energy landscape enhances diffusion within conformational basins but preserves the overall structure and barriers that define the conformational ensemble.

III. APPROXIMATING THE SIDE CHAIN FREE ENERGIES

The benefits of running dynamics with the coarse grained \bar{V} enter at great cost because using even three coarse-grained states per side chain implies a summation over 3^N $\tilde{\chi}$ -states in Eq. 4. Furthermore, the vast majority

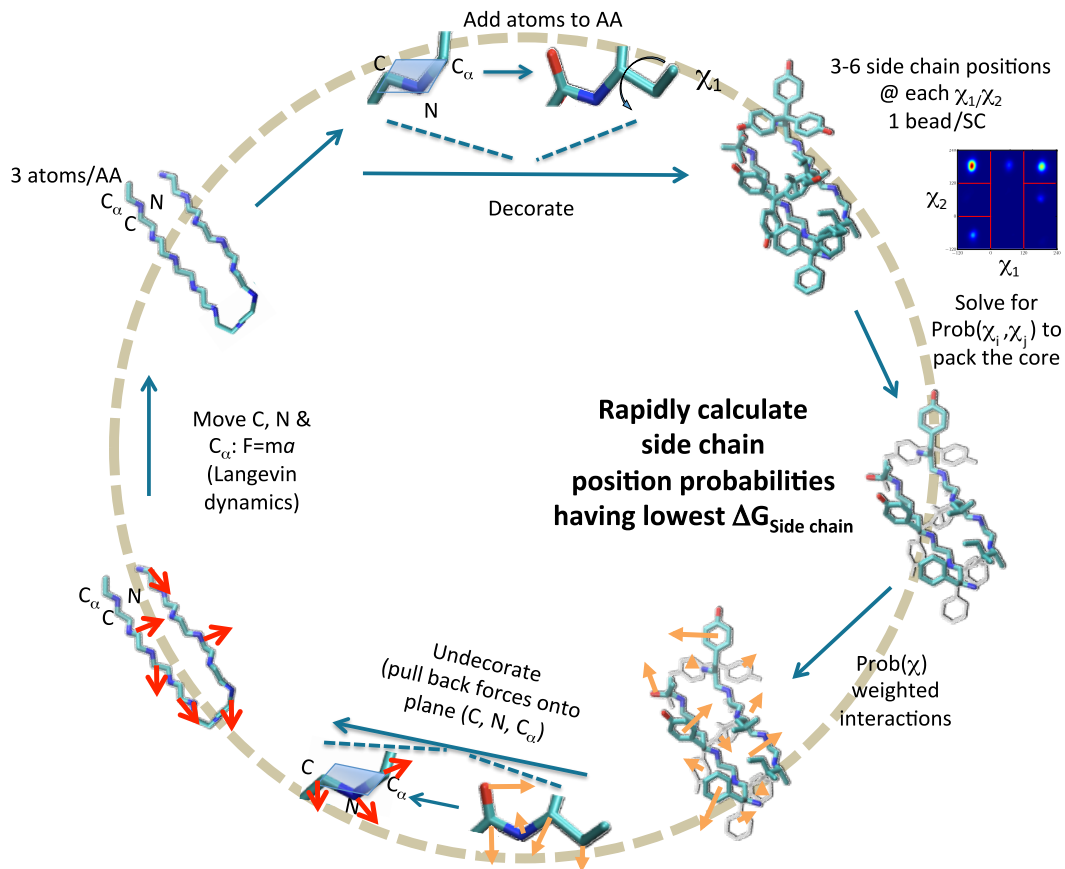


FIG. 1. Inner loop of Upside calculation. The side chain potential enters into the integration step simply as a complicated, many-body energy function that may be treated with standard techniques of molecular simulations.

of those 3^N states have steric clashes or other large energies and, therefore, contribute little to the free energy of the side groups.

To approximate the free energy of the side chains \bar{V} , we express the problem in the language of Ising models so that we can apply standard techniques developed in that context. For a fixed backbone configuration $\{b_i\}$,

$$\begin{aligned} \tilde{V}(\{b_i\}, \{\tilde{\chi}_i\}) &= \bar{v}(\{\tilde{\chi}_i\}) \\ &= \sum_i v_i^{(1)}(\tilde{\chi}_i) + \sum_{i,j}^{\text{neighbors}} v_{ij}^{(2)}(\tilde{\chi}_i, \tilde{\chi}_j), \quad (5) \end{aligned}$$

where the potentials \bar{v} are written in lowercase to indicate suppression of the dependence on the fixed backbone coordinates $\{b_i\}$ in order to focus on the side chain contribution. Notice that with the backbone positions fixed, each single-residue potential $v_i^{(1)}$ is simply a vector with as many components as the number of possible states for $\tilde{\chi}_i$ (e.g. length-6 vectors). Similarly, each of the pair potentials $v_{ij}^{(2)}$ is a small 6x6 matrix of potential energies to cover a maximum of 36 possibilities. These single and pair potentials are calculated only once before evaluating the free energy as described in section IV. Moreover, the pair summation in Eq. 5 only applies for residues pairs i

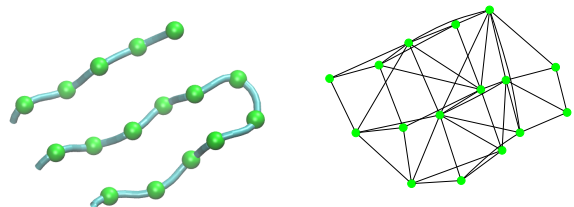


FIG. 2. Fragment of protein G with associated interaction graph ($R_{\text{cutoff}} = 7\text{\AA}$). A pair of residues has a connection whenever their side chain beads are within R_{cutoff} for any side chain states.

and j that are neighbors spatially. A pair of residues (i, j) are neighbors if inter-residue distance $|y_i(\tilde{\chi}_i) - y_j(\tilde{\chi}_j)|$ is less than a cutoff R_{cutoff} for any of their possible discrete states $(\tilde{\chi}_i, \tilde{\chi}_j)$. In this work, we use $R_{\text{cutoff}} = 7\text{\AA}$ for side chain-side chain interactions and $R_{\text{cutoff}} = 5\text{\AA}$ for side chain-backbone interactions.

The potential \tilde{V} may be visualized as an energy function on a graph with one discrete site per amino acid. The graph has a connection between any two residues that are within the cutoff separation R_{cutoff} (Figure 2). The structure of this graph varies dynamically over the

course of a simulation because the definition of neighboring residues depends on the backbone configuration $\{b_i\}$. The potential varies smoothly as the backbone moves so long as the pairwise potential functions are continuous in the backbone coordinates. The potential \tilde{V} is continuous despite the changing connections of the graph because the strength of the potential for each interaction approaches zero at R_{cutoff} just before the connection is eliminated from the graph. Problems such as this, with discrete potentials on an arbitrary graph, are extensively studied in both statistical mechanics (as variants of the Ising model) and machine learning (as undirected graphical models or Markov random fields)⁶. Below we adopt some well studied approximations from these fields to provide accurate and tractable methods for computing our coarse-grain potential \tilde{V} .

Two approximations (see reference 6) are invoked to compute the free energy from

$$\tilde{V} = G^{\text{SC}} = -\log \sum_{\tilde{\chi}_1, \dots, \tilde{\chi}_N} e^{-v(\{\tilde{\chi}_i\})}. \quad (6)$$

The first approximation is to express the free energy G^{SC} in terms of the entropy and average energy of the Boltzmann ensemble where the entropy has been replaced by an approximation,

$$\begin{aligned} G^{\text{SC}} &= \langle \bar{v} \rangle - S \\ &\approx \langle \bar{v} \rangle - S^{\text{approx}}, \end{aligned} \quad (7)$$

where $\langle \bar{v} \rangle$ and S^{approx} are defined in Eq. 8 and Eq. 9. We express the average energy and approximate entropy using the single-residue probabilities $p_i(\tilde{\chi}_i)$ that residue i is in state $\tilde{\chi}_i$ in the Boltzmann ensemble of \bar{v} and similarly for the joint probabilities $p_{ij}(\tilde{\chi}_i, \tilde{\chi}_j)$. Using p_i and p_{ij} , the approximate energy and entropy are

$$\begin{aligned} \langle \bar{v} \rangle &= \sum_i \sum_{\tilde{\chi}_i} p_i(\tilde{\chi}_i) v_i^{(1)}(\tilde{\chi}_i) + \\ &\quad \sum_{\substack{i,j \\ \text{neighbors}}} \sum_{\tilde{\chi}_i, \tilde{\chi}_j} p_{ij}(\tilde{\chi}_i, \tilde{\chi}_j) v_{ij}^{(2)}(\tilde{\chi}_i, \tilde{\chi}_j) \end{aligned} \quad (8)$$

$$\begin{aligned} S^{\text{approx}} &= \sum_i \sum_{\tilde{\chi}_i} p_i(\tilde{\chi}_i) (-\log p_i(\tilde{\chi}_i)) - \\ &\quad \sum_{\substack{i,j \\ \text{neighbors}}} \sum_{\tilde{\chi}_i, \tilde{\chi}_j} p_{ij}(\tilde{\chi}_i, \tilde{\chi}_j) \log \frac{p_{ij}(\tilde{\chi}_i, \tilde{\chi}_j)}{p_i(\tilde{\chi}_i) p_j(\tilde{\chi}_j)}. \end{aligned} \quad (9)$$

The mutual information approximation to the entropy ignores contributions from three-residue and higher correlations.

We intend to minimize the approximate free energy in Eq. 7 over all putative Boltzmann probability distributions for the side chain states $\{\tilde{\chi}_i\}$. Notice that only the 1-side chain probabilities p_i and 2-side chain probabilities p_{ij} are required to compute the average energy and

approximate entropy; we do not need the more complicated full joint probability distribution of the $\{\tilde{\chi}_i\}$ states for all side chains. In addition to the mutual information approximation of the entropy, we assume that any pair probability p_{ij} represents possible pair probabilities from a Boltzmann distribution, so that the only task is to minimize the free energy with respect to the pair probabilities. The only constraints imposed are that they must satisfy the obvious consistency conditions for probabilities,

$$p_j(\tilde{\chi}_j) = \sum_{\tilde{\chi}_i} p_{ij}(\tilde{\chi}_i, \tilde{\chi}_j) = \sum_{\tilde{\chi}_k} p_{jk}(\tilde{\chi}_k, \tilde{\chi}_j) \quad (10)$$

$$\sum_{\tilde{\chi}_i, \tilde{\chi}_j} p_{ij}(\tilde{\chi}_i, \tilde{\chi}_j) = 1 \quad (11)$$

$$p_{ij}(\tilde{\chi}_i, \tilde{\chi}_j) = p_{ji}(\tilde{\chi}_j, \tilde{\chi}_i). \quad (12)$$

However, use of only conditions in Eq. 10–12 is insufficient to ensure that a joint probability distribution exists for all the variables consistent with the choices of p_i and p_{ij} . As an explicit example,

$$p_{12} = p_{23} = \begin{pmatrix} 1/3 & 0 & 0 \\ 0 & 1/3 & 0 \\ 0 & 0 & 1/3 \end{pmatrix} \quad (13)$$

$$p_{13} = \begin{pmatrix} 1/9 & 1/9 & 1/9 \\ 1/9 & 1/9 & 1/9 \\ 1/9 & 1/9 & 1/9 \end{pmatrix} \quad (14)$$

obeys conditions Eq. 10–12 but is not representable by any probability distribution on the three residues. This aspect is a result of residue 1 being completely correlated to residue 2, and residue 2 being completely correlated to residue 3, but residues 1 and 3 being independent, which is mathematically impossible. Though this non-representability problem is a potential concern, we expect that it will not be a large source of error.

Accepting the two approximations for entropy and representability, the free energy becomes

$$G^{\text{SC}} \approx \min_{\{p_i\}, \{p_{ij}\}} (\langle \bar{v} \rangle - S^{\text{approx}}). \quad (15)$$

Thus, we now have a tractable approximation to free energy of the side chain. We can minimize that free energy using a self-consistent iteration technique called belief propagation (Appendix A). The iteration typically converges rapidly, often in 10-20 steps.

Molecular dynamics simulations require calculations of the forces on the backbone coordinates, $-\frac{d\tilde{V}}{db_i}$. The forces are obtained from the derivatives of the potential computed using the chain rule. We take advantage of several terms being zero because the pair probabilities minimize

the free energy,

$$\begin{aligned}
\frac{dG^{\text{SC}}}{db_k} &= \frac{\partial G^{\text{SC}}}{\partial b_k} + \sum_i \frac{\partial G^{\text{SC}}}{\partial p_i} \frac{\partial p_i}{\partial b_k} + \sum_{\substack{i,j \\ \text{neighbors}}} \frac{\partial G^{\text{SC}}}{\partial p_{ij}} \frac{\partial p_{ij}}{\partial b_k} \\
&= \frac{\partial G^{\text{SC}}}{\partial b_k} = \frac{\partial \langle \bar{v} \rangle}{\partial b_k} = \left\langle \frac{\partial \bar{v}}{\partial b_k} \right\rangle \\
&= \sum_i \sum_{\tilde{\chi}_i} p_i(\tilde{\chi}_i) \frac{\partial v_i^{(1)}}{\partial b_k}(\tilde{\chi}_i) + \\
&\quad \sum_{\substack{i,j \\ \text{neighbors}}} \sum_{\tilde{\chi}_i, \tilde{\chi}_j} p_{ij}(\tilde{\chi}_i, \tilde{\chi}_j) \frac{\partial v_{ij}^{(2)}}{\partial b_k}(\tilde{\chi}_i, \tilde{\chi}_j) \quad (16)
\end{aligned}$$

where $\frac{\partial G^{\text{SC}}}{\partial p_i} = \frac{\partial G^{\text{SC}}}{\partial p_{ij}} = 0$ because p_i and p_{ij} are chosen to minimize G^{SC} . The remaining simplifications occur because S^{approx} is independent of the backbone coordinates. While the underlying side chain interactions are pairwise additive and vanish outside the cutoff radius R_{cutoff} , the free energy in equation Eq. 7 is a many-body potential that can interact over arbitrary distances.

Since the approximate free energy due to the side chains is not a convex function of the probabilities, local minima may arise and impair the self-consistent iteration from finding the global minimum. To reduce the danger posed by the presence of local minima, calculations are begun from a carefully initialized state (see Appendix A for details). Other self-consistent approximations exist for the side group free energy, such as tree-reweighted belief propagation⁷, that are typically less accurate but always converge to the global minimum of their approximate free energy. Another limitation of the present approximation scheme arises when a bi-stable or multi-stable energy landscape is possible for the rotamer states. If well-separated and equally important minima are present for a single backbone configuration in the rotamer free energy surface, the probabilities only converge to a single minimum and thus underestimate the entropy of the side chains. While this does not appear to occur near the native well, we have not extensively searched for special backbone configurations that would result in bi-stable rotamer energies. The characterization of such problematic configurations, likely near free energy barriers, is left to future work.

IV. BEAD LOCATIONS AND INTERACTIONS

Paralleling the necessity of coarse-graining the rotamer states, side chain atoms themselves also require coarse-graining in order to obtain an inexpensive side chain model. This reduction in the number of degrees of freedom is further justified since the atomic positions of the side chains are uncertain due to the discretization and aggregation of the rotamer states, meaning that there is little value in assigning precise positions for all atoms.

We instead use a single oriented bead (location and direction coordinates) to represent each side chain (note that the direction is independent of the side chain, e.g. in aromatic residues it could be the ring normal unit vector). The locations and directions of the side chain beads are changed by the optimizer during the optimization of the potential. The improvement in prediction accuracy from using optimized side chain positions rather than the static positions is surprisingly substantial.

We use a combination of isotropic and directional interactions for each pair of interacting side chain or backbone types. The isotropic interactions are primarily responsible for enforcing excluded volume, while the directional interactions typically reflect specific chemical interactions arising from polar groups or aromatic ring stacking. Concretely, each interaction pair is described by positions y_1 and y_2 and directions n_1 and n_2 . From this the distance $r_{12} = |y_1 - y_2|$ and displacement unit vector $n_{12} = (y_1 - y_2)/r_{12}$ are calculated. The form of the interaction is given by

$$V = \kappa(\text{unif}(r_{12}) + \text{ang}_1(-n_1 \cdot n_{12}) \text{ang}_2(n_2 \cdot n_{12}) \text{dir}(r_{12})), \quad (17)$$

where unif , ang_1 , ang_2 , and dir are smooth curves represented by cubic splines.

For side chain-side chain interactions the κ prefactor is 1, but for side chain-backbone interactions κ depends on the hydrogen bonding state of the backbone residue. This distinction reflects that the presence of one hydrogen bond inhibits the formation of another due to competition for the lone pair of electrons. Specifically, the interaction between a backbone hydrogen or oxygen is given a hydrogen bond confidence score f , a number that is typically close to 0 for non-hydrogen bonded and 1 for hydrogen bonded residues. We set $\kappa = 1 - f$ so that the interaction is only turned on for hydrogens or oxygens that are not participating in a backbone-backbone hydrogen bond. The physical motivation is that the directional interaction primarily describes the effects of the dipole interactions, and in a hydrogen bond the C=O and N-H dipoles have approximately zero total dipole moment. While it is theoretically possible for the algorithm to carefully balance hydrogen and oxygen interactions that themselves cancel out on hydrogen bonded pairs, it is much easier to achieve a physically reasonable model if we enforce the zeroing of directional interactions with already hydrogen-bonded pairs. The hydrogen bond distance and angular criteria are detailed in section S2.

The side chain-backbone interactions are needed to describe helix capping, where a side chain atom forms a hydrogen bond with an otherwise unsatisfied donor or acceptor at the end of helix. We have observed that a proper description of these capping effects is required to avoid helix fraying and inordinately long helices. Harper and Rose⁸ have observed that N-terminal capping of a helix by side chains is more likely to be observed than is C-terminal capping by the side chain. This finding

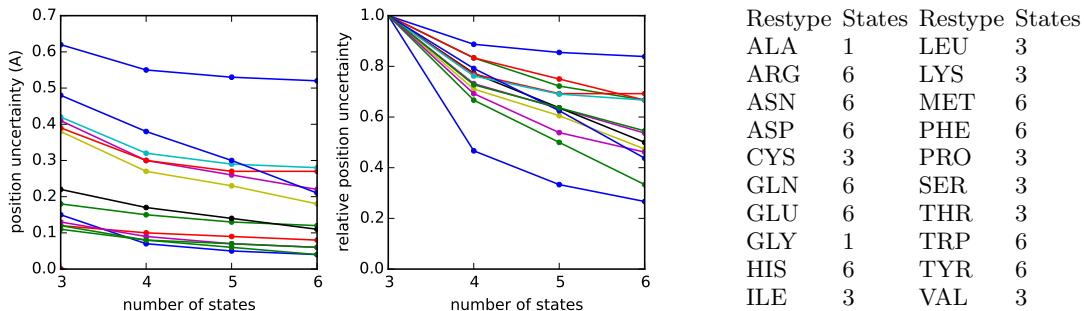


FIG. 3. Error in the decomposition of rotamer states into coarse-grained states as a function of the number of side chain states. The table summarizes the number of states chosen for each amino acid type. The uncertainty in position is σ . The relative uncertainty is the position uncertainty for each number of states divided by the accuracy at three states. One, three or six rotamer states are used, depending on the residue type. For residues without a rotatable χ_2 , such as valine, only three states are needed. The computational time to compute the pairwise interactions and solve for the free energy scales roughly as the number of coarse rotamer states squared, so the use as fewer coarse states is preferred.

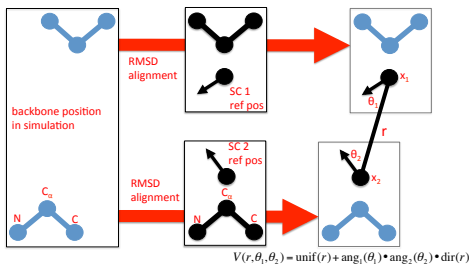


FIG. 4. Coordinates used for side chain interactions. For each residue, a reference backbone structure is aligned to the N, C_α , and C atomic coordinates. This alignment creates a reference frame to establish the position and direction of the side chain bead. The two side chain beads x_1 and x_2 for a pair of residues establishes three coordinates, the distance r and angles θ_1 and θ_2 .

is consistent with our maximum-likelihood training (below), where side chain-amide hydrogen interactions are fit with stronger (i.e. higher confidence) potentials than side chain-oxygen interactions. Harper and Rose also note that hydrophobic residues play a strong role in helix capping by covering the exposed protein backbone at the ends of helices. To provide our model with the freedom to describe this effect, an additional side chain-backbone interaction is added with three beads representing the hydrophobic portion of the backbone. The location of the three beads are initialized from the reference position of N, C_α , and C and are optimized with the rest of the parameters. For this interaction, $\kappa = 1$.

V. MAXIMUM-LIKELIHOOD TRAINING

A. Training objective function

The side chain model is trained by the maximum-likelihood principle. Specifically, we determine the set

of parameters that maximizes the log probability of the true side chain states $\tilde{\chi}_p$ in the Boltzmann ensemble of all possible side chain states $\tilde{\chi}$ for the fixed backbone positions X_p for each protein p .

$$p(\tilde{\chi}_p) = \frac{e^{-V(\tilde{\chi}_p)}}{\sum_{\tilde{\chi}} e^{-V(\tilde{\chi})}} \quad (18)$$

$$-\log p(\tilde{\chi}_p) = V(\tilde{\chi}_p) + \log \left(\sum_{\tilde{\chi}} e^{-V(\tilde{\chi})} \right) \quad (19)$$

$$= V(\tilde{\chi}_p) - G^{\text{SC}} \quad (20)$$

$$= E_{\text{gap}}. \quad (21)$$

The evaluation of E_{gap} requires the evaluation of the free energy of the side chains, a quantity that is intractable to calculate exactly. Fortunately, our side chain energy Eq. 15 approximates the true side chain free energy G^{SC} that appears in Eq. 20. Furthermore, the expression for the parametric derivative Eq. 16 allows for gradient descent optimization to minimize the average gap energy.

B. Training results

The accuracy of the results are computed in two ways. The first measure computes the accuracy of the one-residue probabilities at predicting the χ_1 states of the protein. This quantity is the traditional accuracy measure for side chain packing algorithms. The second measure is the quality of the ensemble, obtained by computing the difference between the free energy of the side chain system and the potential energy of the crystallographic rotamer configuration. For a highly accurate side chain ensemble, we would expect that the crystal configuration would be a high probability state in the ensemble and thus this energy gap would be small. This energy gap is minimized by the maximum-likelihood training. The

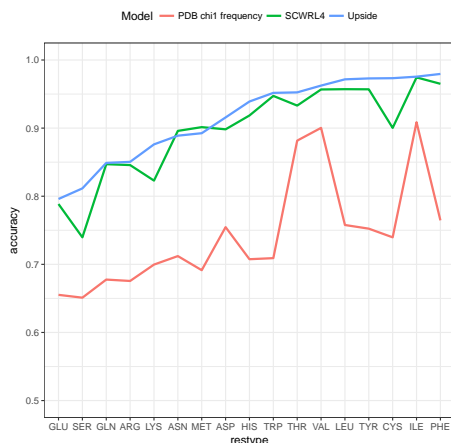


FIG. 5. Comparison of χ_1 prediction accuracy for Upside and SCWRL4, ordered by Upside accuracy. The “PDB χ_1 frequency” line represents the accuracy of the NDRD rotamer library without any interactions; this library is used in both Upside and SCWRL4.

two accuracy measures are typically linearly related for the side chain models we consider.

To compare to state-of-the-art side chain prediction methods, we compare to SCWRL4⁴ on its training and validation set of side chain conformations, as well as the RASP algorithm⁵ for rapid side chain packing. Since the Upside model lacks full side chains, we use the most likely χ_1 rotamer state according to the 1-residue marginal distributions $p_i(\tilde{\chi}_i)$. As per SCWRL4’s validation procedure, the side chains with less than 25th percentile electron density are excluded. To avoid biasing the comparison toward Upside, the SCWRL4 set of proteins is split so that 20% of the proteins are withheld for measuring accuracy, while the rest are used for maximum-likelihood training of Upside. The accuracy metric chosen is to calculate the fraction of side chains for which the Upside or SCWRL4 predicted χ_1 rotamer state agrees with the crystallographic conformation. The residues alanine, glycine, and proline are excluded from the comparison.

The importance of various interactions may be examined directly in Upside by noting the change in accuracy upon their modification. For example in Table I, we can see that using only repulsive interactions causes a 3.8% drop in side chain prediction accuracy compared to the full model, which quantifies the importance of the attractive interactions.

Upside is very accurate, predicting the correct χ_1 rotamer 91.0% of the time using 10 Å cutoffs, which is significantly better than either SCWRL4⁴ or RASP⁵ (Fig 6). Additionally, Upside predicts side chains 16 times faster than the speed-optimized RASP and 300 times faster than accuracy-optimized SCWRL4. This very fast performance enables Upside’s side chain model to be viable in the inner loop of molecular dynamics, as discussed in the next section.

Parameters	Accuracy change (%)	ΔE_{gap} ($k_B T$)
10Å cutoffs	+0.7	-0.028
Full model	0.0	0.000
No H/O interactions	-0.6	0.013
No N,C α ,C beads	-2.3	0.040
ϕ, ψ -independent $V(\chi)$	-3.3	0.004
Isotropic only	-3.5	0.080
Repulsive only	-3.8	0.060
Side chain–side chain only	-3.8	0.067
Side chain–backbone only	-6.1	0.125
No interactions	-13.7	0.435

TABLE I. The significances of various components of the model reflect the decrease in accuracy for their removal. The parameters are separately optimized for each row of the table so that each E_{gap} represents the best achievable for the indicated functional form. Note that these predictions are based on single-chain structures, so they differ slightly in accuracy from the predictions on all-chain structures reported in Figure 6.

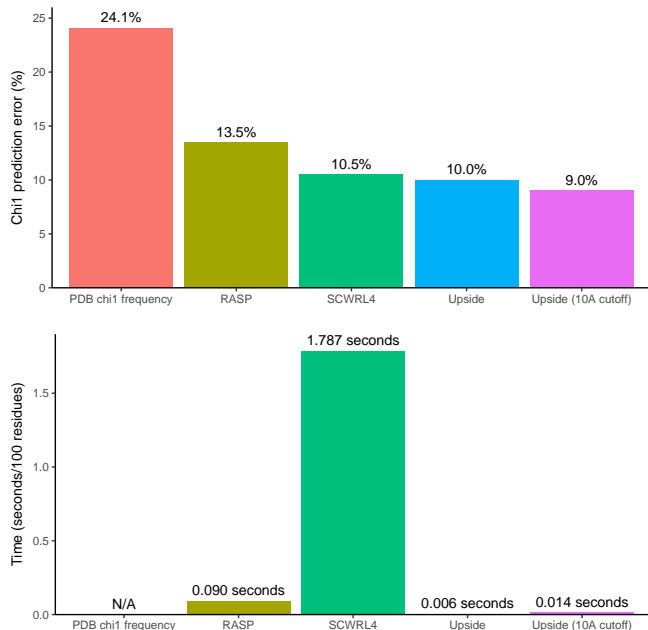


FIG. 6. Comparison of accuracy of predicting side chains with high electron density as well as execution. For all programs, time spent reading the protein structure and writing the results is excluded from the execution time to focus on the cost of solving for the side chain positions. For Upside (10 Å cutoff), all side chain interactions with backbone or other side chains are cutoff at 10 Å.

VI. MOLECULAR DYNAMICS

The parameters obtained from the maximum-likelihood training are optimized for side chain packing for a set of fixed, native backbones. In the limit that the model is flexible enough to model the true side chain interactions and there is unlimited training data, the maximum-likelihood method would recover the true side

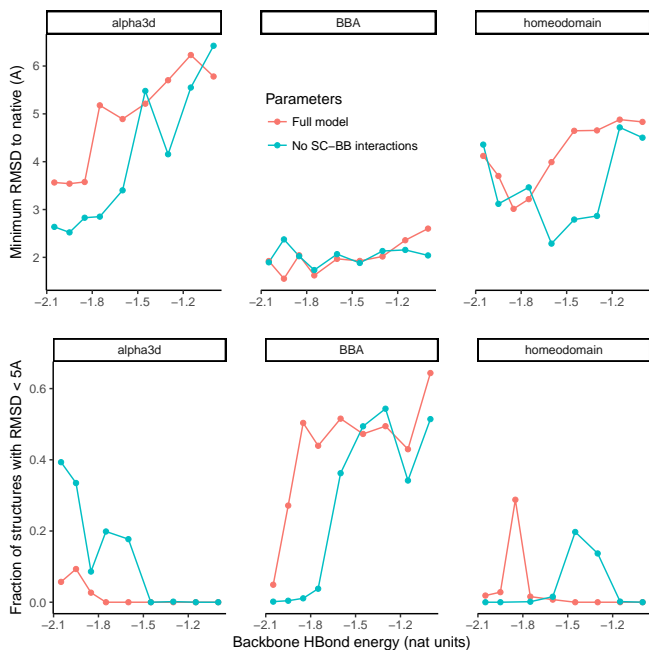


FIG. 7. Accuracy of MD simulations for three proteins at variable backbone hydrogen bond strength. This term does not play an explicit role in the packing optimization as the backbone is fixed. To assign this term an energy, it was manually varied for the best simulation accuracy. This term is the only parameter directly optimized for simulation accuracy.

chain interaction. Even without having the true form of the side chain interaction, the maximum-likelihood parameters assign high probability to the observed rotamer states, thereby including at least some of the underlying physics.

To test the suitability of adapting the side chain packing model to molecular dynamics, simulations were run on small, fast-folding proteins. To create a reasonable protein dynamics model, backbone springs, backbone sterics, hydrogen bond energy, and a basic Ramachandran potential were added to the side chain model (section S2). The Ramachandran potential is derived from a coil library⁹ as a statistical potential. The hydrogen bond enthalpy is varied to find the maximum accuracy. Note that because alanine and glycine have no side chain rotamer states, and hence no training to match the native χ -angles can be conducted, the ALA-ALA, ALA-GLY, and GLY-GLY potentials are completely determined by the regularization. Interactions of ALA and GLY with other residue types are optimized, however, as rotamer states of the other residues provide information on the ALA-X and GLY-X interactions.

VII. RELATED WORK

We highlight several works related to the major features of our model, including molecular dynamics on

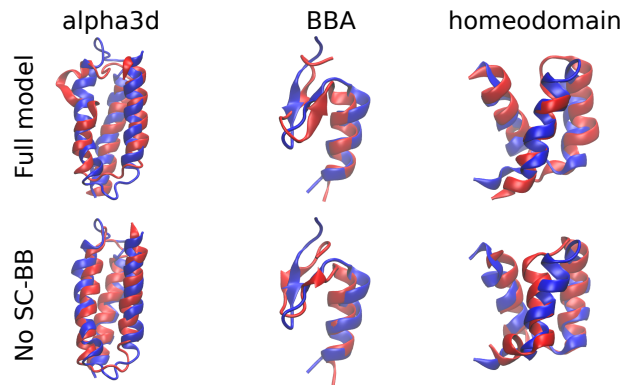


FIG. 8. Closest structure to native for each protein and side chain model at optimal hydrogen bonding strength. Blue is the native structure and red is the simulation.

three atoms but with a dynamic ensemble of side chains, optimized discretization of the side chain states to best represent the protein interactions in the coarse-grained model, a potential with optimized and state-dependent bead locations and orientations, training a protein interaction model for folding using side chain packing accuracy, and a side chain model with an explicit side chain entropy.

A large body of work, exemplified by SCWRL4⁴, has studied the prediction of side chain configurations by discrete rotamer states. SCWRL4 achieves approximately 90% χ_1 accuracy for predicting the most likely rotamer states by minimizing the energy that combines observed rotamer state frequencies and an atomic interaction model⁴. A variety of algorithms have been developed for solving for the highest probability side chain states given the pair interaction values^{10,11}. Kamisetty et al.¹² have worked on scoring protein interaction complexes using a self-consistent approximation to the side chain interactions. Earlier simulation work by Koehl and Delarue¹³ use 1-residue mean field techniques to approximate ensembles of side chain conformations but fail to account for the pairwise correlations of the side chain rotamer states. All of these works use atomically-detailed descriptions of the side chains paired with simple or molecular dynamics interaction terms. Their highly detailed side chains with many χ -angles for each residue make it difficult to perform calculations sufficiently fast for folding simulations, and the use of existing interactions (instead of a newly-trained interaction model) makes it difficult to reduce detail to speed computation. There has also been extensive work in reconstructing backbone positions from side chain beads¹⁴ in lattice models, but these models do not perform a proper summation over possible rotamer states.

RASP⁵ is side chain modeling program designed to significantly improve the speed of side chain packing while achieving comparable accuracy. The authors use careful

selection of the most important energy terms as well as employing clash-detection to guide the optimization of the side chain conformations.

There have also been a large number of coarse-grained techniques that use a variety of non-isotropic potentials for reduced side chain interactions. One of the most successful is the coarse-grained united residue model (UNRES)¹⁵. The model also uses statistical frequencies to determine the positions of the side chains but it emphasizes the parameterization of the coarse-grained model from physics-based calculations instead of statistical information. Though the potential form (Gay-Berne) used in UNRES is quite different from our work, UNRES also uses non-isotropic side chain potentials¹⁶.

Similar to our work, Dama, Sinitskiy, et al.¹⁷ investigate mixed continuous-discrete dynamics, where the states of molecules jump according to a discrete Hamiltonian. Their method differs from our work in a number of important ways: the authors use discrete jumps in state instead of a free energy summation over all states that we employ; they do not optimize the rotamer states as we do; and they train parameters from force matching of molecular dynamics trajectories rather than from the statistical analysis of experimental data as we employ.

VIII. DISCUSSION AND CONCLUSION

We have demonstrated a fast, principled method to coarse-grain discrete side chain states to create a smooth backbone potential. This procedure results in a considerable decrease in computational time as it removes the side chain rattling and friction normally associated with a polypeptide chain moving in a collapsed state. This tracking and instantaneous equilibration of the side chains is analogous to the instantaneously-equilibrated electronic degrees of freedom with respect to the nuclear motions employed in the adiabatic Born-Oppenheimer approximation¹⁸. Motions are calculated only for three heavy backbone atoms, yet the model contains considerable structural detail including hydrogen bonds involving both the backbone and side chains. Further, we have demonstrated both a maximum likelihood procedure to obtain a physically-reasonable potential from the side chain packing of X-ray structures and a tunable discretization of the rotamer states. The resulting method is capable of rapid molecular dynamics sampling of protein structures with moderate accuracy.

The reason that Upside is both faster and more accurate than competing methods at side chain packing is that it shifts the complexity of the χ_1 -prediction problem. Traditional side chain prediction uses a detailed configuration space of all rotamers and side chain atoms but simple interaction forms with few parameters. Upside uses a coarse configuration space with only a single directional bead per residue but a complex and well-optimized set of parameters consisting of over 10,000 jointly-optimized parameters (trained on approximately 500,000 residues).

Upside demonstrates that χ_1 rotamers can be predicted with state-of-the-art accuracy without needing to examine fine-grained atomic packing. Additionally, the side chains in Upside are represented as a Boltzmann ensemble whose 1-residue marginal probabilities are used to predict χ_1 instead of predicting χ_1 using the lowest energy configuration. This approach allows for the natural consideration of side chain entropy and conformational variability. Creating a Boltzmann ensemble over rotamer states also allows exact, continuous forces to be defined for the approximate ensemble, enabling molecular dynamics using potential energies already validated to represent the physics of side chain packing.

A natural question is whether the strengths of SCWRL4 and this algorithm may be combined. There are two reasons to believe that such a combination would be fruitful. The first reason is that when Upside and SCWRL4 predict the same χ_1 rotamer, the prediction is 95.4% accuracy, substantially more accurate than either program alone. This suggests Upside and SCWRL4 provide independent information about the side chain conformations and hence, combining both approaches should produce a substantially better packing model. The second reason that Upside and SCWRL4 may be combined is that Upside provides probability functions as its outputs, rather than just the minimum energy conformation as in SCWRL4. The underlying SCWRL4 single-rotamer energies could be augmented with $-\lambda \log p_{\text{upside}}(\tilde{\chi})$. For an appropriately determined λ , this should incorporate some of Upside’s information directly into SCWRL4, increasing SCWRL4’s accuracy. Alternatively, SCWRL4’s detailed but simple energy function could be augmented by an Upside-style coarse-grained function, possibly with additional maximum-likelihood tuning.

The importance of optimizing the bead locations and directions in our model illustrates the principle that chemical intuition can only be a partial guide to accurate coarse-graining of protein interactions. The location of the interaction sites has a strong effect on our model’s ability to achieve high-packing accuracy, and we expect similarly strong effects would be observed had we directly optimized for backbone conformational accuracy.

For dynamics applications, Upside shows promise as a route to accurate and inexpensive molecular simulation but requires further development. New training techniques are being developed to directly optimize the backbone accuracy of the Upside model. Preliminary results from the new training methods indicates that we are able to achieve dramatic improvements in the accuracy of *de novo* folding while preserving the rapid folding properties. We expect that our belief-propagated side chains will serve as an excellent basis for new methods in protein simulations.

IX. AUTHOR CONTRIBUTIONS

J.M.J. invented algorithm, designed research, performed research, analyzed results, and wrote manuscript. K.F.F. designed research and wrote manuscript. T.R.S. designed research, analyzed results, and wrote manuscript.

ACKNOWLEDGMENTS

This research is supported, in part, by National Science Foundation (NSF) Grant No. CHE-1363012, NIH grant GM 55694, and by the NIGMS of the National Institutes of Health under award number T32GM008720. This work was completed in part with resources provided by the University of Chicago Research Computing Center.

We would like to thank Sheng Wang and Jinbo Xu for helpful discussions during this research. Zhichao Miao kindly provided a modified version of RASP to measure only the side chain packing time.

- ¹J. J. Skinner, W. Yu, E. K. Gichana, M. C. Baxa, J. R. Hinshaw, K. F. Freed, and T. R. Sosnick, *Proceedings of the National Academy of Sciences* **111**, 15975 (2014).
- ²H. M. Berman, J. Westbrook, Z. Feng, G. Gilliland, T. N. Bhat, H. Weissig, I. N. Shindyalov, and P. E. Bourne, *Nucleic acids research* **28**, 235 (2000).
- ³T. Hamelryck, M. Borg, M. Paluszewski, J. Paulsen, J. Frellsen, C. Andreetta, W. Boomsma, S. Bottaro, and J. Ferkinghoff-Borg, *PLoS one* **5**, e13714 (2010).
- ⁴G. G. Krivov, M. V. Shapovalov, and R. L. Dunbrack, *Proteins: Structure, Function, and Bioinformatics* **77**, 778 (2009).
- ⁵Z. Miao, Y. Cao, and T. Jiang, *Bioinformatics* **27**, 3117 (2011).
- ⁶M. J. Wainwright and M. I. Jordan, *Foundations and Trends® in Machine Learning* **1**, 1 (2008).
- ⁷M. J. Wainwright, T. S. Jaakkola, and A. S. Willsky, in *AISTATS* (2003).
- ⁸E. T. Harper and G. D. Rose, *Biochemistry* **32**, 7605 (1993).
- ⁹D. Ting, G. Wang, M. Shapovalov, R. Mitra, M. I. Jordan, and R. L. Dunbrack Jr, *PLoS Comput Biol* **6**, e1000763 (2010).
- ¹⁰J. Desmet, M. D. Maeyer, B. Hazes, and I. Lasters, *Nature* **356**, 539 (1992).
- ¹¹J. Xu and B. Berger, *Journal of the ACM (JACM)* **53**, 533 (2006).
- ¹²H. Kamisetty, E. P. Xing, and C. J. Langmead, *Journal of Computational Biology* **15**, 755 (2008).
- ¹³P. Koehl and M. Delarue, *Journal of molecular biology* **239**, 249 (1994).
- ¹⁴M. Feig, P. Rotkiewicz, A. Kolinski, J. Skolnick, and C. L. Brooks, *Proteins: Structure, Function, and Bioinformatics* **41**, 86 (2000).
- ¹⁵A. Liwo, J. Pillardy, C. Czaplewski, J. Lee, D. R. Ripoll, M. Groth, S. Rodziewicz-Motowidlo, R. Kamierkiewicz, R. J. Wawak, S. Oldziej, *et al.*, in *Proceedings of the fourth annual international conference on Computational molecular biology* (ACM, 2000) pp. 193–200.
- ¹⁶A. K. Sieradzian, P. Krupa, H. A. Scheraga, A. Liwo, and C. Czaplewski, *Journal of chemical theory and computation* **11**, 817 (2015).
- ¹⁷J. F. Dama, A. V. Sinititskiy, M. McCullagh, J. Weare, B. Roux, A. R. Dinner, and G. A. Voth, *Journal of Chemical Theory and Computation* **9**, 2466 (2013).
- ¹⁸M. Born and R. Oppenheimer, *Annalen der Physik* **389**, 457 (1927).

- ¹⁹J. S. Yedidia, W. T. Freeman, and Y. Weiss, *Exploring artificial intelligence in the new millennium* **8**, 236 (2003).
- ²⁰G. Wang and R. L. Dunbrack, *Bioinformatics* **19**, 1589 (2003).
- ²¹M. A. Fischler and R. C. Bolles, *Communications of the ACM* **24**, 381 (1981).
- ²²J. K. Salmon, M. A. Moraes, R. O. Dror, and D. E. Shaw, in *2011 International Conference for High Performance Computing, Networking, Storage and Analysis (SC)* (IEEE, 2011) pp. 1–12.
- ²³D. Kingma and J. Ba, arXiv preprint arXiv:1412.6980 (2014).
- ²⁴M. Abadi, A. Agarwal, P. Barham, E. Brevdo, Z. Chen, C. Citro, G. S. Corrado, A. Davis, J. Dean, M. Devin, S. Ghemawat, I. Goodfellow, A. Harp, G. Irving, M. Isard, Y. Jia, R. Jozefowicz, L. Kaiser, M. Kudlur, J. Levenberg, D. Mané, R. Monga, S. Moore, D. Murray, C. Olah, M. Schuster, J. Shlens, B. Steiner, I. Sutskever, K. Talwar, P. Tucker, V. Vanhoucke, V. Vasudevan, F. Viégas, O. Vinyals, P. Warden, M. Wattenberg, M. Wicke, Y. Yu, and X. Zheng, “TensorFlow: Large-scale machine learning on heterogeneous systems,” (2015), software available from tensorflow.org.
- ²⁵M. V. Shapovalov and R. L. Dunbrack, *Structure* **19**, 844 (2011).

Appendix A. BELIEF PROPAGATION

For convenience, this appendix contains a brief description of the equations used to implement belief propagation for the side chain free energies. Given 1-residue energies $v_i(\tilde{\chi}_i)$ and 2-residue energies $v_{ij}(\tilde{\chi}_i, \tilde{\chi}_j)$, we seek probabilities $p_i(\tilde{\chi}_i)$ and $p_{ij}(\tilde{\chi}_i, \tilde{\chi}_j)$ to minimize the free energy in Eq. 15.

It is helpful to first understand the intuition behind the belief propagation process. We seek a consistent set of 1- and 2-side chain probabilities for the residues compatible with the interaction potential Eq. 5. The probability of each residue state $\tilde{\chi}_i$ for residue i is determined by two factors. The first factor is the 1-residue energy $v_i(\tilde{\chi}_i)$ that would determine the probabilities exactly in the absence of interactions. The second factor is consistency with the side chain states of the residues in contact with residue i , where consistency is determined by the potentials $v_{ij}(\tilde{\chi}_i, \tilde{\chi}_j)$. Belief propagation optimizes these factors to minimize the approximate free energy Eq. 15 as derived in reference 19. The iteration is described more formally below, including a damping term λ to suppress oscillations during the self-consistent iteration.

For 1-residue beliefs, define $b_i^r(\tilde{\chi}_i)$ to be the round r “belief” that the i -th residue is in state $\tilde{\chi}_i$. For the 2-residue beliefs, we have two beliefs for each pair of interacting residues (i.e. any pair of residues that interact in any rotamer states). Define $b_{ij}^r(\tilde{\chi}_j)$ to be the round r belief for the residue pair (i, j) that residue j is in state $\tilde{\chi}_j$. The belief $b_{ji}^r(\tilde{\chi}_i)$ is defined similarly.

To initialize the algorithm at round 0, we take

$$b_i^0(\tilde{\chi}_i) = e^{-v_i(\tilde{\chi}_i)} \quad (22)$$

$$b_{ji}^0(\tilde{\chi}_i) = \sum_{\tilde{\chi}_j} e^{-v_{ij}(\tilde{\chi}_i, \tilde{\chi}_j)} b_j^0(\tilde{\chi}_j). \quad (23)$$

We compute the round $r + 1$ beliefs from the round r

beliefs according to the following equations.

$$b_{ji}^{r+1}(\tilde{\chi}_i) = \sum_{\tilde{\chi}_j} e^{-v_{ij}(\tilde{\chi}_i, \tilde{\chi}_j)} \frac{b_j^r(\tilde{\chi}_j)}{b_{ij}^r(\tilde{\chi}_j)} \quad (24)$$

$$b_i^{r+1}(\tilde{\chi}_i) = \lambda b_i^r(\tilde{\chi}_i) + (1 - \lambda) \frac{e^{-v_i(\tilde{\chi}_i)} \prod_j b_{ji}^{r+1}(\tilde{\chi}_i)}{\sum_{\tilde{\chi}_i} e^{-v_i(\tilde{\chi}_i)} \prod_j b_{ji}^{r+1}(\tilde{\chi}_i)} \quad (25)$$

The products in Eq. 24 should be understood as taken only over residues j that interact with residue i . The damping constant λ suppresses oscillatory behavior that hinders convergence ($\lambda = 0.4$ is used in the present work). The equations are iterated until $|b_i^{r+1}(\tilde{\chi}_i) - b_i^r(\tilde{\chi}_i)| < 0.001$ for all residues i and states $\tilde{\chi}_i$.

From the converged beliefs $b_i(\tilde{\chi}_i)$ and $b_{ij}(\tilde{\chi}_j)$, we can compute the marginal probabilities

$$p_i(\tilde{\chi}_i) = b_i(\tilde{\chi}_i) \quad (26)$$

$$p_{ij}(\tilde{\chi}_i, \tilde{\chi}_j) = \frac{\frac{b_i(\tilde{\chi}_i)}{b_{ji}(\tilde{\chi}_i)} e^{-v_{ij}(\tilde{\chi}_i, \tilde{\chi}_j)} \frac{b_j(\tilde{\chi}_j)}{b_{ij}(\tilde{\chi}_j)}}{\sum_{\tilde{\chi}_i, \tilde{\chi}_j} \frac{b_i(\tilde{\chi}_i)}{b_{ji}(\tilde{\chi}_i)} e^{-v_{ij}(\tilde{\chi}_i, \tilde{\chi}_j)} \frac{b_j(\tilde{\chi}_j)}{b_{ij}(\tilde{\chi}_j)}}. \quad (27)$$

The free energy of the model is obtained by using the marginal probabilities above in Eq. 15.

(SUPPLEMENTAL INFORMATION ON NEXT PAGE)

Supplemental Information

S1. TRAINING SET

The side chain packing interaction is trained using a large, non-redundant collection of crystal structures from the PDB with 50–500 residues and resolution less than 2.2Å. From a training set of protein structures, we extract the sequences s_p , backbone trace positions X_p , and true coarse-grained side chain states $\tilde{\chi}_p$ for each protein p . The proteins are further filtered using PISCES²⁰ so that all pairs of proteins have sequence similarity less than 30%. Non-globular structures in the dataset are removed, as we suspect that the side chain packing of these structures is more strongly influenced by other chains in the crystal structures. We define non-globular structures as outliers in the linear relationship between $\log(N_{\text{res}})$ and $\log(R_g)$; the outliers are identified using the RANSAC algorithm²¹. After filtering, 6255 chains remained, containing approximately 1.4 million residues.

S2. SIMULATION DETAILS

Name	PDB ID	Length	Sequence
alpha3d	2a3d	73	MGSWAEFKQLRAAIKTRLQALGGSEAEALAA FEKEIAAFESSELQAYKKGKGNPEVEALRKEA AAIRDQLQAYRHN
BBL	2wxc	47	GSQNNDALSPAIRRLLAEWNLDAIAIKGTG VGGRLTREDVEKHLAKA
homeodomain	2p6j	52	MKQWSENVEEKLKEFVKRHRITQEELHQY AQRLLGNEEAIRQFFEEFEQRK

TABLE S1. Sequences of proteins for molecular dynamics

All simulations are run with Upside, a custom simulation engine that implements the belief propagation of side chain interactions as well as the parameter derivatives needed for gradient descent.

The replica exchange temperatures are 0.500, 0.532, 0.566, 0.600, 0.636, 0.672, 0.709, 0.748, 0.787, 0.828, 0.869, 0.912, 0.955, and 1.000. The Ramachandran potential uses the NDRD TCB coil library⁹. The backbone hydrogen bond interaction uses both distance and angle criteria to determine hydrogen bonds. The H-O bond distance interaction starts at approximately 1.4Å and ends at 2.5Å. Both the N-H-O and H-O-C criteria half-heights are at approximately 47 degrees off of collinear.

We use Verlet integration with a time step of 0.009 units. We use the random number generator Random123²² to implement the Langevin dynamics with a thermalization time scale of 0.135 time units. The thermalization time scale (related to Langevin friction) is chosen to maximize the effective diffusion rate of chains while effectively controlling simulation temperature. As Langevin dynamics with any friction coefficient produces the same Boltzmann ensemble, we chose to maximize equilibration of our system rather than attempt to match a solvent viscosity.

The cutoff radius for side chain-side chain interactions is 7Å, and the cutoff radius for side chain-backbone interactions is 5Å. The distance splines are zero-derivative-clamped cubic splines with a knot spacing of 0.5Å. The angular splines have a knot spacing of 0.167 in $\cos\theta$, which ranges over $[-1, 1]$.

S3. OPTIMIZATION DETAILS

The Adam optimizer²³ is used to minimize the energy gap. This optimizer is convenient because it automatically adjusts the gradient descent step size for each parameter according to the typical scale of the gradient in that dimension. This rescaling is important because spline coefficients at large radii tend to have much larger gradient magnitudes than parameters at small radii.

We use the following settings for the Adam optimizer: minibatch size 256 proteins, $\alpha = 0.03$, $\beta_1 = 0.90$, $\beta_2 = 0.96$, $\epsilon = 10^{-6}$. Positivity constraints on the angular coefficients are enforced by an exponential transform. The regularization integrals over all space are approximated by sums at the knot locations of the radial and angular splines.

A regularization penalty is added to the maximum-likelihood optimization that encourages smoothness of the potential. This penalty also reduces the validation error of the training. The regularization penalties chosen are

$$\sum_i (2c_i^{\text{unif}} - c_{i-1}^{\text{unif}} - c_{i+1}^{\text{unif}})^2 \quad (\text{S1})$$

$$\sum_i (c_i^{\text{dir}})^2 \quad (\text{S2})$$

$$\sum_i (c_0^{\text{unif}} - (5 k_B T))^2 \quad (\text{S3})$$

The penalty Eq.S1 encourages a small second derivative for the isotropic (unif) term, while the penalty Eq.S2 minimizes the size of the directional interactions. Finally, the penalty Eq.S3 ensures a strong steric core for interactions.

The derivative calculations needed for regularization and coordinate transforms are handled with the Tensorflow framework²⁴.

S4. OPTIMIZED MAPPING TO COARSE STATES

The χ -angles for the side chains are partitioned into discrete states in an optimized manner. The NDRD rotamer library²⁵ provides a set of approximate discrete states for each residue type according to their frequencies of occurrence in a non-redundant set of high resolution

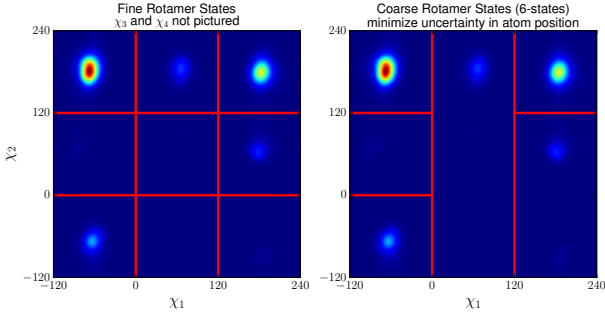


FIG. S1. Example of optimized coarse states for arginine overlaid on the PDB distribution of the rotamer angles χ_1 and χ_2 . Each of the six coarse states contains only a single fine state that has high probability, so that the variance of dihedral angles within each coarse state is small.

protein structures in the PDB. However, the number of rotamer states in the NDRD library can be quite large. For instance, naively using all 81 rotamers for each arginine means that computing the pair interaction $v_{i,j}$ for two arginines would require computing $81^2 = 6561$ energy values. Consequently, instead of using all possible rotamer states, several NDRD rotamer states are combined into 3–6 coarse-grained rotamer states for the sake of manageable computational cost.

We choose to aggregate the rotamer states of the side chain to minimize the positional uncertainty of side chain atoms in each state. A search over all possible aggregations is conducted to find the aggregation that provides the smallest possible error. More formally, the NDRD rotamer library²⁵ is used to define the atomic positions $x_{ij}^f(\phi, \psi)$, where i is the atom (such as C_β), j is the coordinate (x , y , or z), and f is the fine-grained rotamer state. Each rotamer state has a probability $p^f(\phi, \psi)$ specified in the NDRD library from frequencies in the PDB for each fine-grained rotamer state as a function of the backbone dihedral angles (ϕ, ψ) . Each fine-grained state f may belong to exactly one coarse-grained state c (i.e. the c states form a partition of the f states). Given the choice of a coarse-grained state c , an average is performed over the fine-grained atomic positions, and sum is taken over the probabilities of all fine-grained states f grouped into c according to the prescription,

$$q^c(\phi, \psi) = \sum_{f \in c} p^f(\phi, \psi) \quad (\text{S4})$$

$$y_{ij}^c(\phi, \psi) = \frac{1}{q^c(\phi, \psi)} \sum_{f \in c} p_{ij}^f(\phi, \psi) x_{ij}^f(\phi, \psi), \quad (\text{S5})$$

where q^c is the coarse-grained probability and y_{ij}^c is the coarse-grained atomic position.

The error incurred by coarse-graining is defined as the variance of the atom positions within each coarse-grained

state, weighted by the frequency of occurrence of the coarse-grained state in the PDB. Specifically, the error $\sigma^2(\phi, \psi)$ is defined as,

$$\sigma^2(\phi, \psi) = \sum_f \frac{p^f(\phi, \psi)}{N_{\text{atom}}} \sum_{ij} (x_{ij}^f(\phi, \psi) - y_{ij}^{c(f)}(\phi, \psi))^2, \quad (\text{S6})$$

where N_{atom} is the number of atoms in the side chain and $c(f)$ is the coarse-grained state c that contains the fine-grained state f . The error depends implicitly on the state decomposition $c(f)$ and measures the deviation of the atoms within each state. This error favors the fine-grained states f that occur with higher frequency in the PDB.

The division of fine-grained states into coarse-grained states is restricted for simplicity to be independent of the Ramachandran angles for the residue,

$$\sigma^2 = \int p^{\text{Rama}}(\phi, \psi) \sigma^2(\phi, \psi) d\phi d\psi, \quad (\text{S7})$$

where $p^{\text{Rama}}(\phi, \psi)$ is the frequency of each Ramachandran angle taken from the PDB coil library. Note that this error term depends implicitly on the decomposition $c(f)$ and weights for the (ϕ, ψ) pairs according to their frequencies in the coil library.

An optimal coarse-grained representation of the side chain rotamer states is obtained by minimizing σ^2 for each residue type over all partitions $c(f)$. We force the coarse-graining $c(f)$ to obey a few conditions, essentially to make sure that $c(f)$ is easily interpretable in terms of χ_1 and χ_2 as well as limiting the number of possibilities that must be checked by the brute-force minimization. In particular, the mapping from coarse states back to χ_1 rotamer states is unambiguous because no single coarse state contains two different χ_1 rotamer states. We impose the following conditions:

1. $c(f)$ depends only on the χ_1 and χ_2 rotamer states of f (i.e. if f_1 and f_2 states differ only in their χ_3 or χ_4 states, then $c(f_1) = c(f_2)$).
2. Each coarse state c must contain only a single χ_1 state but may contain multiple distinct χ_2 states for that χ_1 state.
3. Each coarse state c must contain a contiguous range of χ_2 values. This greatly reduces the number of possible coarse-grainings for residues with non-rotameric χ_2 angles like asparagine.

We optimize the decomposition of the coarse-grained state $c(f)$ by completely enumerating all possible decompositions into coarse-grained states that satisfy the three conditions above and contain no more than six coarse states.